Available online at www.sciencedirect.com
ScienceDirect
Ceramics International 35 (2009) 1027–1032
CERAMICS INTERNATIONAL
www.elsevier.com/locate/ceramint

Characterization of strontium aluminate phosphors prepared from milled $SrCO_3$

Yu-Lun Chang [a], Hsing-I. Hsiang [a,*], Ming-Tsai Liang [b]

[a] *Particulate Materials Research Center, Department of Resources Engineering, National Cheng Kung University, No. 1, University Road, Tainan City 701, Taiwan, ROC*
[b] *Department of Chemical Engineering, I-Shou University, No. 1, Section 1, Syuecheng Road, Dashu Township, Kaohsiung County 840, Taiwan, ROC*

Received 16 July 2007; received in revised form 10 February 2008; accepted 17 April 2008
Available online 12 July 2008

Abstract

$SrAl_2O_4:Eu^{2+},Dy^{3+}$ phosphors were prepared by solid-state reaction from milled $SrCO_3$. The effect of milling treatment of $SrCO_3$ on the formation and physical properties of $SrAl_2O_4$ phosphors was investigated by DTA, XRD, BET, SEM and PL. The results indicate that small crystallite size and large specific surface area of the milled $SrCO_3$ were able to increase the contact points between the reactants and to reduce the average transport distance for materials diffusion. Therefore, the solid-state reaction can be accelerated and the formation of $SrAl_2O_4$ was facilitated. On the other hand, the number of nucleation sites was also suggested to be increased that leads to a decrease in $SrAl_2O_4$ crystallite size and an increase in specific surface area. The increased specific surface area was proposed to increase the emission intensity and afterglow decay.

Keyword : A. Powders: solid-state reaction

1. Introduction

Rare earth ions-doped strontium aluminate, $SrAl_2O_4:Eu^{2+},Dy^{3+}$, is an important material for long-persistent luminescence. $SrAl_2O_4$ has a stuffed tridymite structure, which is constructed by corner-shared AlO_4 tetrahedrons, and large divalent cations, Sr^{2+} ions, to occupy the interstitial sites to compensate the charge imbalance [1]. Since the ionic radii are similar, doped Eu^{2+} ions and Dy^{3+} ions are suggested to substitute Sr^{2+} sites within the stuffed tridymite structure. The 4f–5d transition of Eu^{2+} ions in the $SrAl_2O_4$ matrix provides a broad band emission centered at about 520 nm [2]. Dy^{3+} is a co-activator, which can trap holes from the 4f–5d transition of Eu^{2+} ions, thereby leading to long-persistent luminescence [3].

The solid-state reaction from α-Al_2O_3 and $SrCO_3$ is the most widely used method to prepare $SrAl_2O_4$ [4,5]. In this process, the intermediate species, $Sr_3Al_2O_6$, which is detrimental to the phosphorescence, is often formed due to the difficulty for material diffusion. To remove it, the sample needs to be calcined at higher temperatures. Song et al. observed that $SrAl_2O_4$ and $Sr_3Al_2O_6$ are stable phases at 1000 °C, and the transformation of these phases into pure $SrAl_2O_4$ requires calcination at a higher temperature of 1250 °C [6]. Recently, Chen et al. used the high-energy ball milling treatment to prepare $SrAl_2O_4$. They proposed that the reaction between Al_2O_3 and $SrCO_3$ towards $SrAl_2O_4$ could be partially activated after milling for 5–30 h. Therefore, the formation of $Sr_3Al_2O_6$ was suppressed and a nearly pure phase of $SrAl_2O_4$ can be obtained at a rather low temperature of around 900 °C [7]. In addition, they also prepared $BaAl_2O_4$ using the high-energy ball milling treatment from Al_2O_3 and $BaCO_3$. Pure $BaAl_2O_4$ can be obtained at 900 °C for 2 h [8].

In this study, to obtain pure $SrAl_2O_4$ phosphors by solid-state reaction at lower temperatures, $SrCO_3$ was ball milled for various times before mixing with other reactants. The effects of the ball milling treatment on the character of $SrCO_3$ and the formation and physical properties of $SrAl_2O_4$ were investigated using DTA, XRD, BET, TEM, SEM and PL.

2. Experimental

Commercial $SrCO_3$ (Aldrich, 99.9%) was milled using the ball milling treatment with 5 mm zirconia media in ethanol at

* Corresponding author. Tel.: +886 6 2757575x62821; fax: +886 6 2380421.
E-mail address: hsingi@mail.ncku.edu.tw (H.-I. Hsiang).

0272-8842/$34.00.
doi:10.1016/j.ceramint.2008.04.022

250 rpm for 2, 6, and 12 h, respectively. Then the milled carbonates were mixed with α-Al_2O_3 (Alfa Aesar, 99.9%), Eu_2O_3 (Acros, 99.9%) and Dy_2O_3 (Prochem, 99.99%) in a stoichiometric ratio as $Sr_{0.97}(Eu_{0.01})(Dy_{0.02})Al_2O_4$ by further ball milling for 4 h. After 120 °C drying, the dried mixtures were calcined at various temperatures with a heating rate of 10 °C/min. The calcinations were carried out in 95% N_2–5% H_2 atmosphere.

The thermal behavior of these mixtures was recorded by DTA (Netzsch, STA 409 PC) with a heating rate of 10 °C/min and air flow rate of 40 mL/min. XRD (Siemens, D5000) with Cu-Kα radiation (λ = 1.5406 Å) was used to analyze the crystalline phases, crystallite sizes and the internal strains of samples.

The crystallite sizes were calculated using Scherrer's equation:

$$D_{hkl} = \frac{0.9\lambda}{B \times \cos\theta} \quad (1)$$

where $D_{h\,k\,l}$ is the crystallite size, λ is 1.5406 Å, θ is the diffraction angle, and β is the full width at half maximum (FWHM).

Internal strains of the milled specimens can be approximated using the Hall equation from the XRD information [9]:

$$\frac{\beta \times \cos\theta}{\lambda} = \frac{1}{D_{hkl}} + \varepsilon_{hkj}\frac{\sin\theta}{\lambda} \quad (2)$$

where $\varepsilon_{h\,k\,l}$ is the internal strain and $D_{h\,k\,l}$ is the effective crystallite size.

The specific surface areas were measured by BET (Micromeritics, ASAP 2020). SEM (Hitachi, S4100) and TEM (Jeol, JEM-3010) were used to observe the particle sizes and morphologies of samples. The powder size distribution (PSD) and the mean particle size (d_{50}) were calculated using the equivalent projected area diameter determination and selected over 150 particles according to SEM photographs. PL spectrometer (Hitachi, F-4500) was employed to measure the luminescent properties of resultant samples.

3. Results and discussion

3.1. Characterization of $SrCO_3$

Fig. 1 shows TEM photographs of the $SrCO_3$ particles after milling for various times. It is observed that un-milled $SrCO_3$ (as milling for 0 h) had a pillar-like shape with length of about 0.5 μm. By increasing the milling time, the pillar-like shape diminished and the particle size decreased gradually. In addition, the particle size distribution also became broadened. For milling time of up to 12 h, the $SrCO_3$ transformed into many tiny particles with size smaller than 0.3 μm and showed a rather broad particle size distribution. Fig. 2 shows XRD patterns of these particles. All of them are identified as orthorhombic $SrCO_3$ (JCPDS 05-0418). However, the crystal-

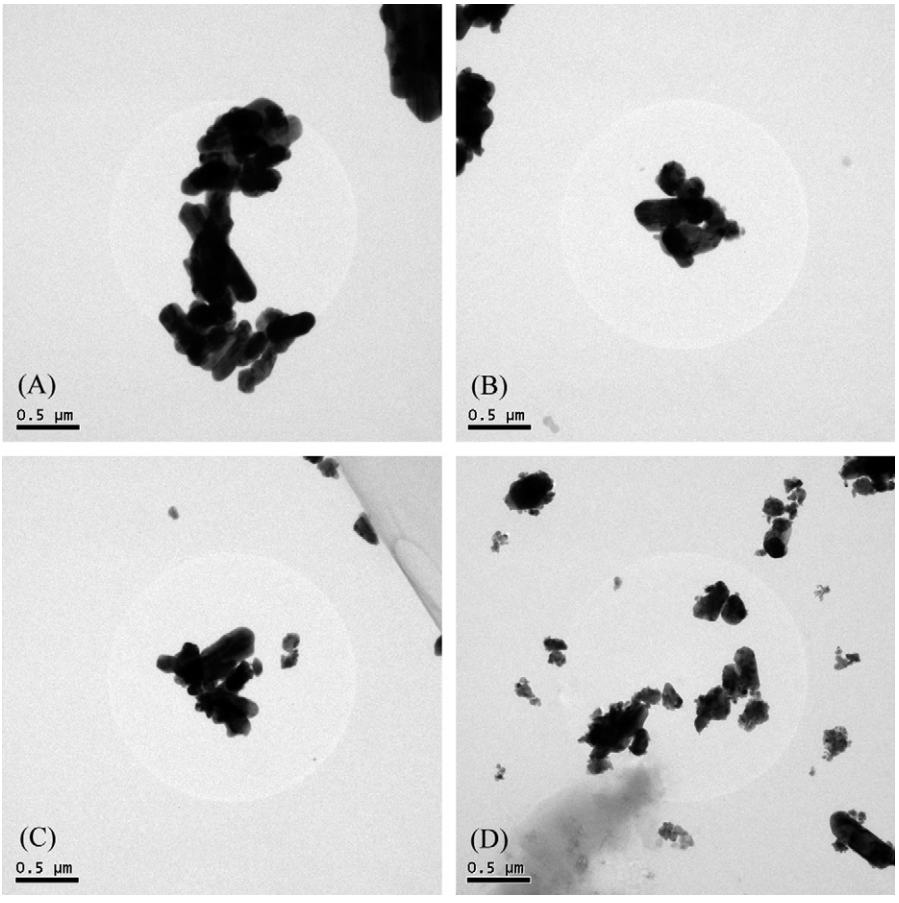

Fig. 1. TEM photographs of the $SrCO_3$ particles after milling for various times, (A) 0 h, (B) 2 h, (C) 6 h, and (D) 12 h.

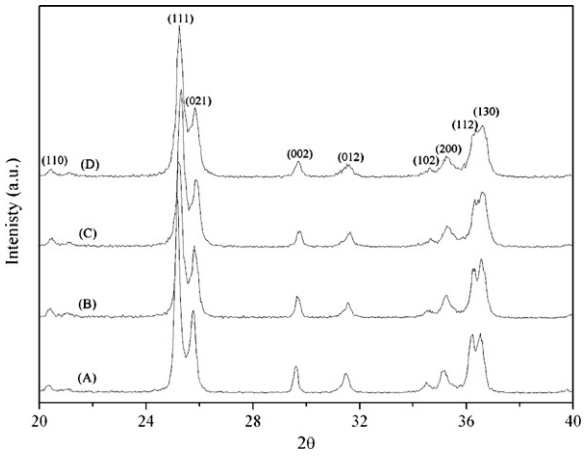

Fig. 2. XRD patterns of the $SrCO_3$ particles after milling for various times, (A) 0 h, (B) 2 h, (C) 6 h, and (D) 12 h.

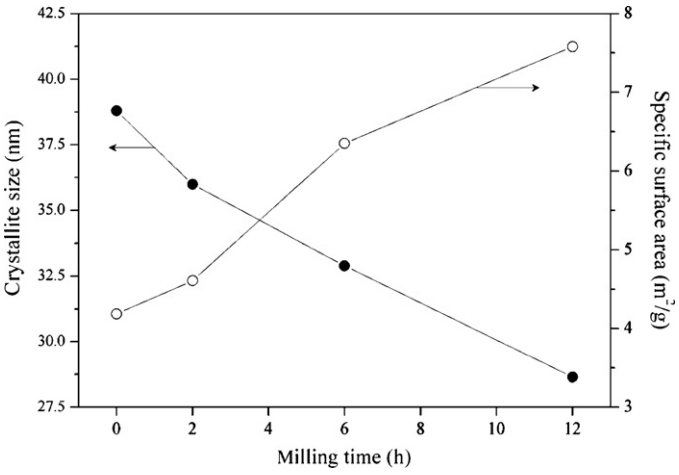

Fig. 3. Crystallite size from Scherrer's calculation on (1 1 1) and specific surface areas of the $SrCO_3$ particles after milling for various times.

linity seems to decrease with an increase of the milling time. According to Scherrer's calculation of FWHM on (1 1 1), the crystallite size of $SrCO_3$ decreased from 38.79 nm to 28.65 nm by increasing the milling time from 0 h to 12 h (as shown in Fig. 3.). Besides, the specific surface areas of $SrCO_3$ show an increasing tendency with the milling time.

Based on Hall's estimation, the fitting results gave the same slopes (~0.09) for un-milled and 12 h-milled $SrCO_3$ in the sin θ vs. $\beta \cos\theta/\lambda$ plots (Fig. 4), indicating that they had identical internal strains ($\varepsilon_{h\ k\ l}$) in the crystal lattice. Therefore, the ball milling treatment of $SrCO_3$ was suggested to fragment the particles without generating extra internal strains in the $SrCO_3$ lattice. It just resulted in a decrease of crystallite size and an increase of specific surface area of $SrCO_3$ particles.

3.2. Formation and physical properties of $SrAl_2O_4$ phosphors

Fig. 5 shows DTA curves of the dried mixtures. There are two obvious peaks on curve (A) in the temperature interval between 900 °C and 1100 °C. According to Sweeney's report,

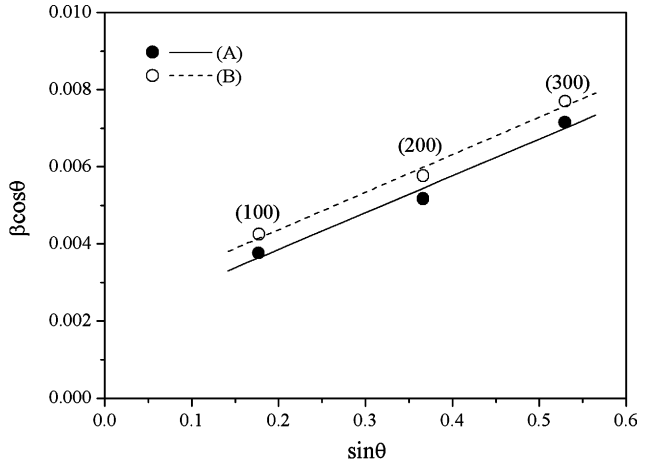

Fig. 4. Hall's approximation of (1 0 0), (2 0 0) and (3 0 0) for the $SrCO_3$ after milling for various times: (A) 0 h and (B) 12 h.

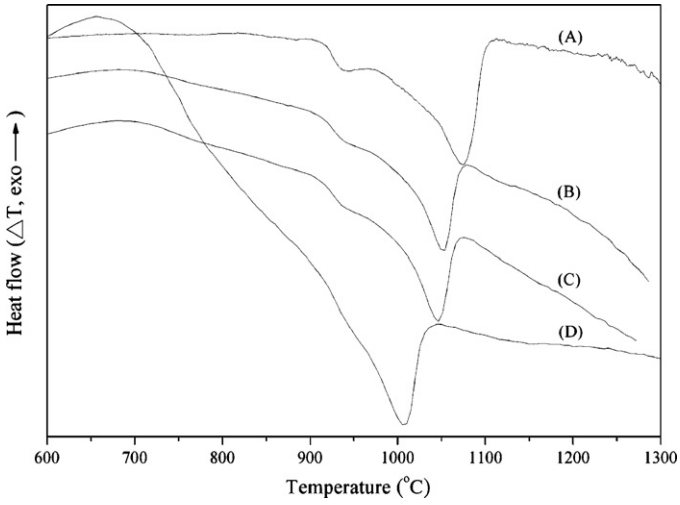

Fig. 5. DTA curves of mixtures mad from $SrCO_3$ after milling for various times: (A) 0 h, (B) 2 h, (C) 6 h, and (D) 12 h.

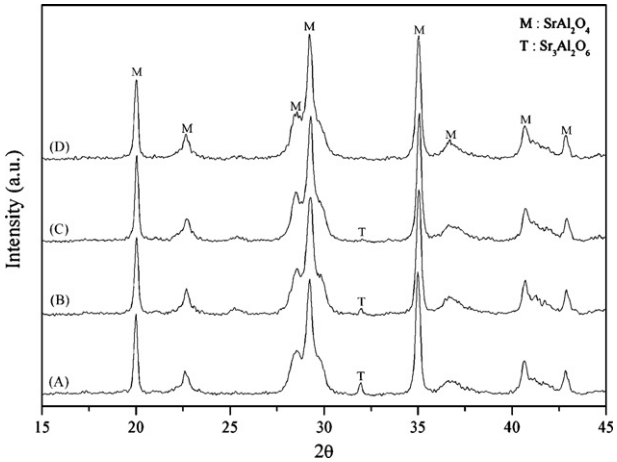

Fig. 6. XRD patterns of samples made from $SrCO_3$ after milling for various times: (A) 0 h, (B) 2 h, (C) 6 h, and (D) 12 h, and calcined at 950 °C for 3 h.

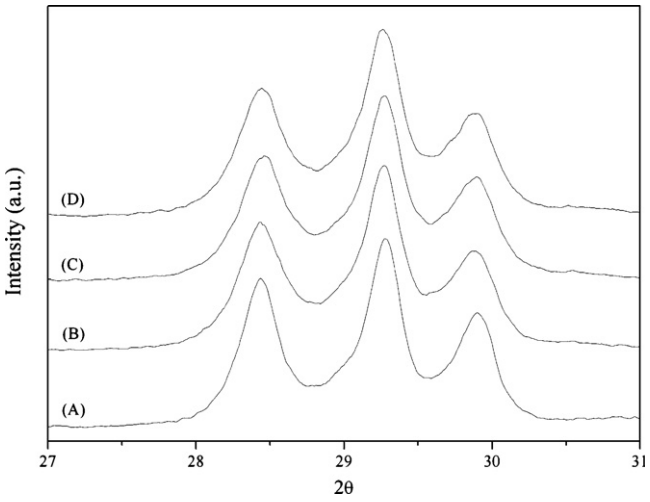

Fig. 7. XRD patterns of samples made from $SrCO_3$ after milling for various times: (A) 0 h, (B) 2 h, (C) 6 h, and (D) 12 h, and calcined at 1100 °C for 4 h.

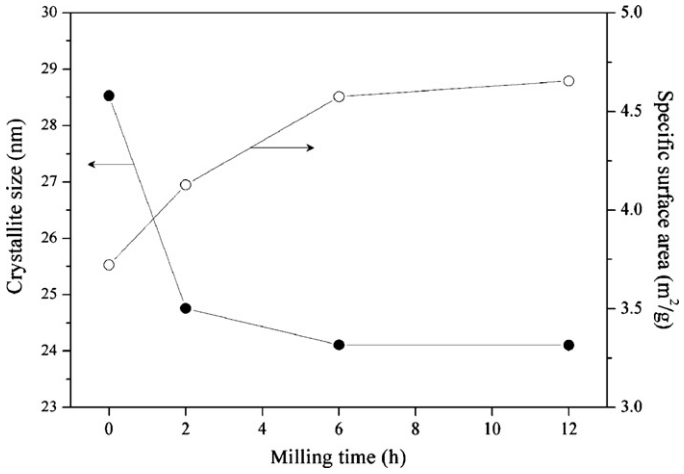

Fig. 8. Crystallite size from Scherrer's calculation on (−2 1 1) and specific surface area of samples made from $SrCO_3$ after milling for various times and calcined at 1100 °C for 4 h.

these two endothermic changes can be attributed to the polymorphic phase transformation (∼920 °C) and the decomposition (950–1100 °C) of $SrCO_3$, respectively [10]. For all mixtures, the first endothermic peaks occurred at the same temperature of around 920 °C, but the peak shape broadened with increasing milling time of $SrCO_3$. It is probably due to the inhomogeneous temperature distribution of $SrCO_3$ with a broadened particle size distribution caused by the ball milling treatment. On the other hand, the second endothermic peak was shifted toward lower temperatures with increasing $SrCO_3$ milling time. For the mixture made from 12 h-milled $SrCO_3$, the second endothermic peak completed at 1050 °C, which is almost 50 °C lower than that using un-milled $SrCO_3$.

Fig. 6 shows XRD patterns of the samples calcined at 950 °C for 3 h. It indicates that these samples consisted of mainly monoclinic $SrAl_2O_4$ (JCPDS 34-0379). Besides, a small amount of $Sr_3Al_2O_6$ (JCPDS 24-1187) decreasing gradually with an increase of the $SrCO_3$ milling time was further observed. For the sample made from 12 h-milled $SrCO_3$, the reflection of $Sr_3Al_2O_6$ almost disappeared and pure monoclinic $SrAl_2O_4$ was obtained. It is suggested that the smaller crystallite size and larger surface area of $SrCO_3$ were able to increase the contact point between the reactants, thereby reducing the average transport distance for material diffusion [11]. As a result, the solid-state reaction can be accelerated and the formation of $SrAl_2O_4$ was facilitated.

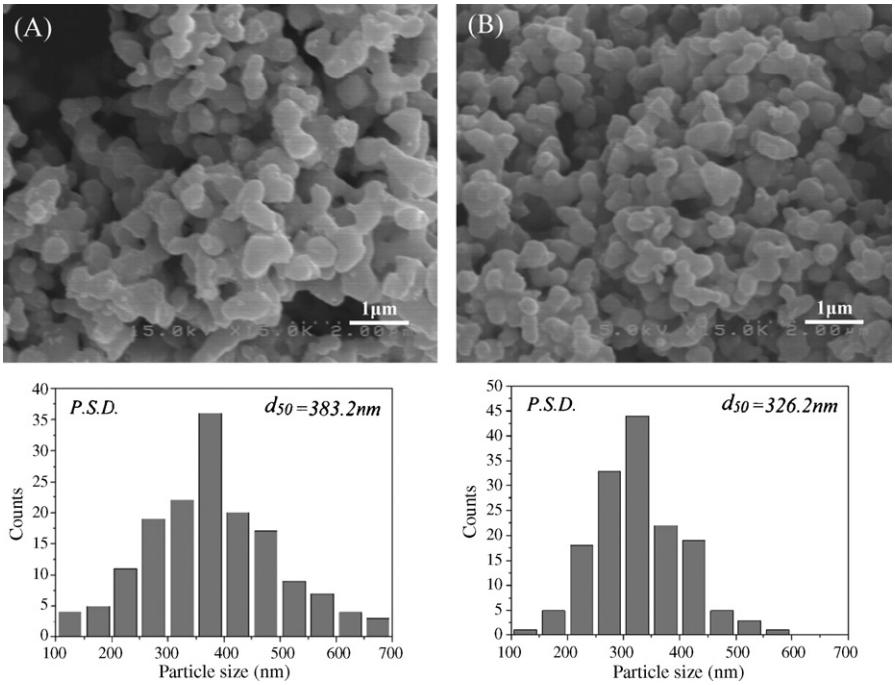

Fig. 9. SEM photographs and size distributions of samples made from $SrCO_3$ after milling for various times: (A) 0 h and (B) 12 h, and calcined at 1100 °C for 4 h.

After calcining at 1100 °C for 4 h, all samples all were pure $SrAl_2O_4$, except for the sample which used un-milled $SrCO_3$ which further showed trace amounts of $Sr_3Al_2O_6$. The XRD peaks of (−2 1 1), (2 2 0) and (2 1 1) of monoclinic $SrAl_2O_4$ are shown in Fig. 7. It is observed that these peaks seem to broaden gradually with increasing $SrCO_3$ milling time. According to Scherrer's calculation of FWHM on (−2 1 1), the crystallite size of $SrAl_2O_4$ decreased slightly from 28.53 nm to 24.08 nm with increasing milling time from 0 h to 12 h (as shown in Fig. 8.). In addition, the specific surface areas of these samples increased from 3.72 m^2/g to 4.65 m^2/g with an increase of the milling time. Fig. 9 shows SEM photographs of the samples using un-milled and 12 h-milled $SrCO_3$. It is observed that the sample prepared using 12 h-milled $SrCO_3$ not only had smaller particle sizes but also showed a narrower particle size distribution. The suppression of grain growth may be resulted from an increase of the number of nucleation sites [12,13]. Nevertheless, the number of nucleation sites is suggested to increase with an increase of the contact point between reactants. Therefore, preparation using milled $SrCO_3$ led to a decrease in $SrAl_2O_4$ crystallite size and an increase in its specific surface area.

Fig. 10 shows PL spectra of the samples calcined at 1100 °C for 4 h. All of them had a broad emission band centered at about 511 nm, which can be attributed to the 4f–5d transition of Eu^{2+} ions in $SrAl_2O_4$. The sample prepared using un-milled $SrCO_3$, due to the presence of traces of $Sr_3Al_2O_6$, showed the weakest emission intensity. By increasing the $SrCO_3$ milling time, the emission intensity increased gradually. Fig. 11 shows the afterglow of these samples. It indicates that the afterglow of the sample using un-milled $SrCO_3$ also decayed most rapidly. The persistent time of other samples seems to increase with an increase of the $SrCO_3$ milling time. The samples made from 12 h-milled $SrCO_3$ showed both the highest initial emission intensity and the longest decay. This can be attributed to an increase in surface trapping levels commensurate with changes in the surface area of the sample [14]. Large specific surface area of the sample was proposed to increase the luminescent and trapping opportunity for Eu^{2+} and Dy^{3+}.

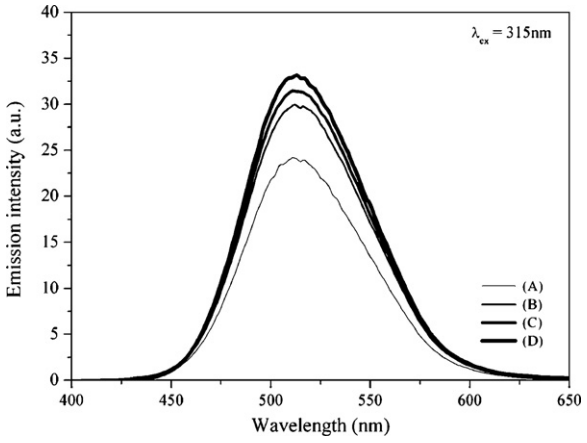

Fig. 10. Emission spectra of samples made from $SrCO_3$ after milling for various times: (A) 0 h, (B) 2 h, (C) 6 h, and (D) 12 h, and calcined at 1100 °C for 4 h.

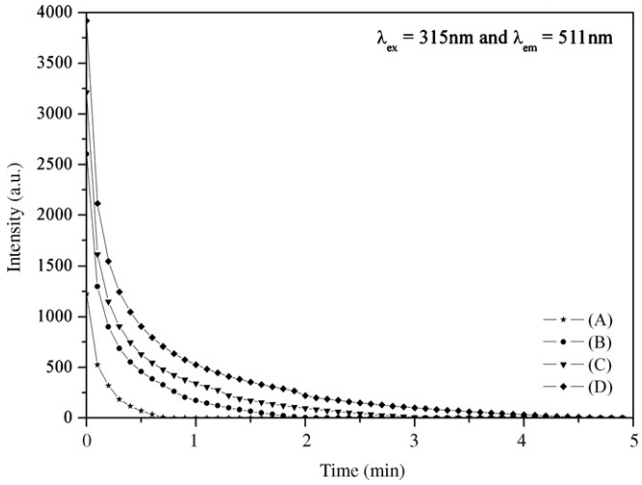

Fig. 11. Afterglow of samples made from $SrCO_3$ after milling for various times: (A) 0 h, (B) 2 h, (C) 6 h, and (D) 12 h, and calcined at 1100 °C for 4 h.

4. Conclusions

$SrCO_3$ with different crystallite size can be obtained by ball milling for various times. The milling treatment only fragmented the particles without generating extra internal strains in the $SrCO_3$ lattice. Small crystallite size and large specific surface area of the milled $SrCO_3$ were suggested to increase the contact points between the reactants and to reduce the average transport distance for materials diffusion. Thus, the formation of $SrAl_2O_4$ in the solid-state reaction was facilitated. Pure phase monoclinic $SrAl_2O_4$ can be obtained even at 950 °C for 3 h for the sample made from 12 h-milled $SrCO_3$. Moreover, the sample prepared made from 12 h-milled $SrCO_3$ and calcined at 1100 °C for 4 h showed the smallest $SrAl_2O_4$ crystallite size, the largest specific surface area and a narrower particle size distribution. This was ascribed to the suppression of grain growth due to an increase of the number of nucleation sites. Furthermore, the increased specific surface area was proposed to increase the emission intensity and afterglow decay.

Acknowledgments

This work was financially co-sponsored by the Ministry of Economic Affairs of the Republic of China through contract (92-EC-17-A-08-S1-023) and National Science Council of the Republic of China (NSC94-2216-E-006-026).

References

[1] F.P. Glasser, L.S.D. Glasser, Crystal chemistry of some AB_2O_4 compounds, J. Am. Ceram. Soc. 46 (1963) 377–380.
[2] S.H.M. Poort, W.P. Blokpoel, G. Blasse, Luminescence of Eu^{2+} in barium and strontium aluminate and gallate, Chem. Mater. 7 (1995) 1547–1551.
[3] T. Matsuzawa, Y. Aoki, N. Takeuchi, Y. Murayama, New long phosphorescent phosphor with high brightness, $SrAl_2O_4$:Eu^{2+},Dy^{3+}, J. Electrochem. Soc. 143 (1996) 2670–2673.
[4] D. Ravichandran, S.T. Johnson, S. Erdei, R. Roy, W.B. White, Crystal chemistry and luminescence of the Eu^{2+}-activated alkaline earth aluminate phosphors, Display 19 (1999) 197–203.

[5] T. Aitasalo, J. Holsa, H. Jungner, M. Lastusaari, J. Niittykoski, Mechanisms of persistent luminescence in Eu^{2+}, RE^{3+} doped alkaline earth aluminates, J. Lumin. 94–95 (2001) 59–63.
[6] Y.K. Song, S.K. Choi, H.S. Moon, T.W. Kim, S.I. Mho, H.L. Park, Phase studies of $SrO–Al_2O_3$ by emission signatures of Eu^{2+} and Eu^{3+}, Mater. Res. Bull. 32 (1997) 337–341.
[7] G. Chen, D. Niu, X. Liu, Preparation of $SrAl_2O_4$ from an oxide mixture via a high-energy ball milling, J. Alloys Compd. 399 (2005) 280–283.
[8] G. Chen, D. Niu, Mechanical activation of barium aluminate formation from $BaCO_3–Al_2O_3$ mixtures, J. Alloys Compd. 413 (2006) 319–322.
[9] Y.Q. Li, J. Xu, T. Qiu, X.C. He, X.M. Sheng, Alumina effect on the phase transformation in vibration ball-milling zirconia(yttria) powders, J. Mat. Sci. Let. 11 (1992) 669–670.
[10] M. Sweeney, Thermal stabilities of isoelectronic, isostructural nitrates, carbonates and borates, Thermochim. Acta 11 (1975) 409–424.
[11] M.T. Buscaglia, M. Bassoli, V. Buscaglia, R. Alessio, Solid-state synthesis of ultrafine $BaTiO_3$ powders from nanocrystalline $BaCO_3$ and TiO_2, J. Am. Ceram. Soc. 88 (2005) 2374–2379.
[12] R. Yanagawa, M. Senna, Preparation of 200 nm $BaTiO_3$ particles with their tetragonality 1.010 via a solid-state reaction preceded by agglomeration-free mechanical activation, J. Am. Ceram. Soc. 90 (2007) 809–814.
[13] C. Ando, R. Yanagawa, H. Chazono, H. Kishi, M. Senna, Nuclei-growth optimization for fine-grained $BaTiO_3$ by precision-controlled mechanical pretreatment of starting powder mixture, J. Mater. Res. 19 (2004) 3592–3599.
[14] X. Wang, Z.Y. He, D. Jia, W. Strekd, R. Pazik, D. Hreniak, W.M. Yen, Crystal size dependence of the persistent phosphorescence in $Sr_2ZnSi_2O_7:Eu^{2+},Dy^{3+}$, Microelectron. J. 36 (2005) 546–548.